

Engineering Symmetry-Selective Couplings of a Superconducting Artificial Molecule to Microwave Waveguides

Mohammed Ali Aamir[✉], Claudia Castillo Moreno[✉], Simon Sundelin, Janka Biznárová, Marco Scigliuzzo[✉], Kowshik Erappaji Patel, Amr Osman, D. P. Lozano[✉], Ingrid Strandberg, and Simone Gasparinetti^{✉†}

Department of Microtechnology and Nanoscience, Chalmers University of Technology, 412 96 Gothenburg, Sweden



(Received 24 February 2022; accepted 8 August 2022; published 15 September 2022)

Tailoring the decay rate of structured quantum emitters into their environment opens new avenues for nonlinear quantum optics, collective phenomena, and quantum communications. Here, we demonstrate a novel coupling scheme between an artificial molecule comprising two identical, strongly coupled transmon qubits and two microwave waveguides. In our scheme, the coupling is engineered so that transitions between states of the same (opposite) symmetry, with respect to the permutation operator, are predominantly coupled to one (the other) waveguide. The symmetry-based coupling selectivity, as quantified by the ratio of the coupling strengths, exceeds a factor of 30 for both waveguides in our device. In addition, we implement a Raman process activated by simultaneously driving both waveguides, and show that it can be used to coherently couple states of different symmetry in the single-excitation manifold of the molecule. Using that process, we implement frequency conversion across the waveguides, mediated by the molecule, with efficiency of about 95%. Finally, we show that this coupling arrangement makes it possible to straightforwardly generate spatially separated Bell states propagating across the waveguides. We envisage further applications to quantum thermodynamics, microwave photodetection, and photon-photon gates.

DOI: 10.1103/PhysRevLett.129.123604

Waveguide quantum electrodynamics (QED) is an emerging field of research that studies the interaction of quantum emitters with waveguides hosting a continuum of one-dimensional photonic modes [1–4]. It has been explored in several experimental platforms that include atoms [5], solid-state quantum defects [6], semiconductor quantum dots [7], and superconducting circuits [8] with either optical or microwave waveguides. A plethora of rich and diverse physics has become accessible from these studies, such as resonance fluorescence [9], nonclassical states of light [10,11], collective effects [5,8,12–18], giant artificial atoms [19–21], chiral photonic transport [22–26], atom-photon bound states [27–30], topological physics [31,32], and tunable non-Markovian dynamics [33,34]. Waveguide QED finds applications in single-photon sources and quantum communication [3], quantum information processing [35], and, recently, quantum thermodynamics [36–39].

The primary aspect in waveguide QED is the tailoring of the coupling mechanisms of quantum emitters to a waveguide. When multiple resonant emitters are involved, they

form collective states known as Dicke states [40]. Their coupling strength depends on the symmetry property of their composite wave function with respect to exchanges of emitters. Depending on the symmetry, Dicke states are either bright or dark states because they emit rapidly or slowly [12,16,41,42]. Owing to their isolated nature, dark states are promising resources for quantum information processing [43–46] and quantum memories [47]. For the same reason, they are also challenging to control or detect [13,14,18]. Quantum control of dark states has been achieved using multiple classical drives with a definite phase relation [18,48].

Here, we present a simple architecture of two superconducting artificial atoms coupled to two microwave waveguides such that each waveguide couples *selectively* to collective states possessing one of the two manifesting symmetries, characterized by the permutation operator. Thus, each collective state of a given symmetry is a dark state to one waveguide but a bright state to the other waveguide, and therefore is independently amenable to both control and detection. We also demonstrate the scope of its applications with two distinct experiments: (1) coupling between a pair of bright and dark states (having opposite symmetries) by activating a Raman process and mediation of coherent population transfers with an efficiency of about 95% [49], thereby also achieving a frequency conversion [50]; (2) generation of spatially

Published by the American Physical Society under the terms of the [Creative Commons Attribution 4.0 International license](#). Further distribution of this work must maintain attribution to the author(s) and the published article's title, journal citation, and DOI. Funded by Bibsam.

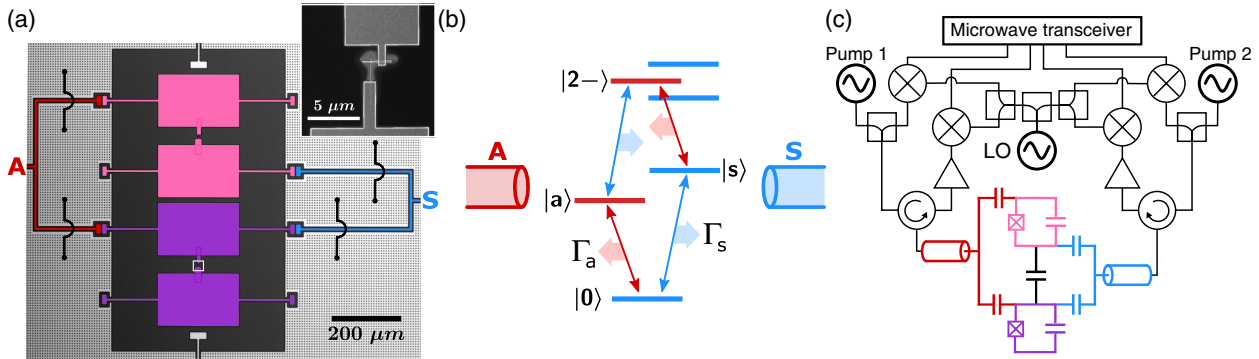


FIG. 1. Device architecture and experimental setup. (a) False-color micrograph of the device comprising two split transmons (pink and violet) coupled to two microwave waveguides labeled A (red) and S (blue). Black wires represent bonding wires connecting isolated islands to the ground plane. A small white box delineates the area containing one of the Josephson junctions, enlarged in the inset. (b) Energy-level diagram of the collective states of the artificial molecule up to the double-excitation manifold. States with odd (even) symmetry, as well as symmetry-inverting (symmetry-preserving) transitions are indicated in red (blue). Symmetry-inverting (symmetry-preserving) transitions predominantly couple to waveguide A (S), as indicated by horizontal arrows. Transitions to doubly excited states other than $|2-\rangle$ are omitted for clarity (shown in Supplemental Material [63]). (c) Simplified experimental setup (LO, local oscillator). See text and Supplemental Material [63].

separated, entangled itinerant photons, in particular a Bell state, employing a simple scheme—a capability [51–54] that is valuable for distributing quantum entanglement [35,55–58].

Our device contains a molecule made of two nominally identical, mutually interacting artificial atoms, each realized with a superconducting transmon [59]. Each transmon has two nodes, made of conducting islands, that form the capacitor and are shunted by a Josephson junction [Fig. 1(a)]. They are coupled to two waveguides in a novel geometry such that the waveguide named A (S) is coupled to the same-side (inner) nodes of each transmon. The Hamiltonian governing the molecule is $\hat{H} = \sum_{i=1,2} (\omega_i \hat{b}_i^\dagger \hat{b}_i + \alpha_i \hat{b}_1^\dagger \hat{b}_1^\dagger \hat{b}_2 \hat{b}_2 / 2) + g(\hat{b}_1^\dagger \hat{b}_2 + \hat{b}_1 \hat{b}_2^\dagger)$, where \hat{b}_i and \hat{b}_i^\dagger are bosonic annihilation and creation operators, ω_i and α_i are the mode transition frequency and the anharmonicity of transmon $i = \{1, 2\}$ respectively, and g is the intertransmon coupling rate [59]. Importantly, the Hamiltonian is invariant under the exchange of constituent atoms; therefore, it commutes with the permutation operator [60–62], whose eigenvalues are ± 1 . Thereby, their eigenstates, which yield an eigenvalue -1 ($+1$) with the permutation operator, are antisymmetrical (symmetrical). The molecule's bare modes in the single-excitation manifold, states $|01\rangle$ and $|10\rangle$, are resonant and split by $2g$ into collective states, $|a\rangle = (|01\rangle - |10\rangle)/\sqrt{2}$ and $|s\rangle = (|01\rangle + |10\rangle)/\sqrt{2}$, that are antisymmetrical and symmetrical, respectively [Fig. 1(b)]. The double-excitation manifold has three collective states where one, $|2-\rangle = (|02\rangle - |20\rangle)/\sqrt{2}$, is antisymmetrical while the other two are symmetrical (see Supplemental Material [63]).

Since the spatial extent of the molecule is deep within subwavelength regime compared to the excitation frequencies (see $\omega_{a,s}$ in Table I), it behaves as a lumped element

and therefore, nearly resonant microwave field drives in the waveguides acquire negligible relative phase across the molecule. However, crucially, the oscillating voltage in the molecule's nodes exhibits relative phase differences such that the same-side (inner) nodes are in phase while being π out of phase with the remaining nodes when the molecule is in the antisymmetric (symmetric) state. Therefore, as a result of our engineered coupling geometry, the drive operators corresponding to waveguides A and S, in the rotating frame, are directly proportional to $\hat{b}_A + \hat{b}_A^\dagger$ and $\hat{b}_S + \hat{b}_S^\dagger$, respectively, where $\hat{b}_A = \hat{b}_1 - \hat{b}_2$ and $\hat{b}_S = \hat{b}_1 + \hat{b}_2$. Thus, waveguide A (S) causes dipole moment transitions between the states that is symmetry-inverting (symmetry-preserving) [see transitions in Fig. 1(b) and the matrix elements in Supplemental Material [63]]. For instance, the transition $|0\rangle \leftrightarrow |a\rangle$ ($|0\rangle \leftrightarrow |s\rangle$) couples strongly to waveguide A (S) at a coupling rate Γ_a (Γ_s).

Our experiments are performed with the device at about 9 mK in a dilution refrigerator. Each waveguide is connected to an input line to deliver microwave drives and an output line with linear amplifiers to measure the scattered microwave signals, separated by a circulator [see Fig. 1(c)].

TABLE I. Experimentally found parameter values.

Parameter	Symbol	Value
$ a\rangle$ mode frequency	$\omega_a/2\pi$	5.6981 GHz
$ s\rangle$ mode frequency	$\omega_s/2\pi$	6.2909 GHz
Qubit-qubit coupling	$g/2\pi$	296.4 MHz
$ a\rangle \rightarrow A$ decay rate	$\Gamma_a/2\pi$	0.311 MHz
$ s\rangle \rightarrow S$ decay rate	$\Gamma_s/2\pi$	1.388 MHz
$ a\rangle \rightarrow S$ decay rate	$\Gamma'_a/2\pi$	8.8 kHz
$ s\rangle \rightarrow A$ decay rate	$\Gamma'_s/2\pi$	29.8 kHz

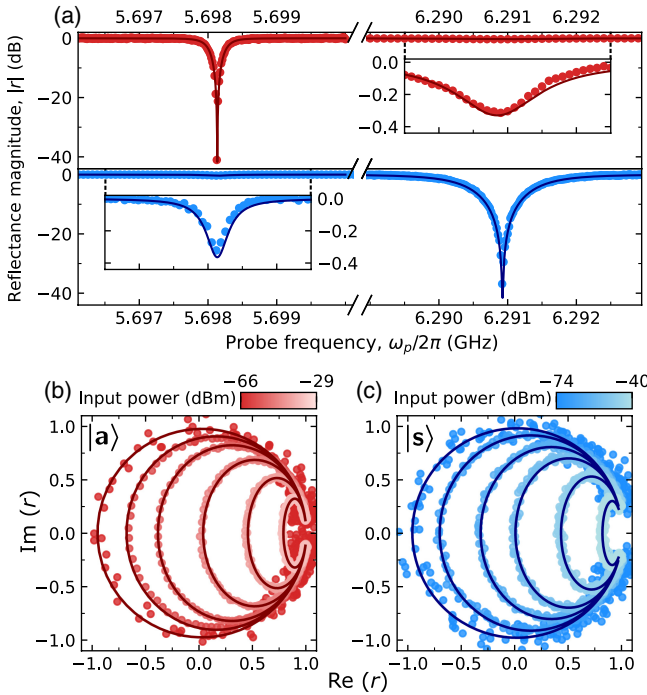


FIG. 2. Reflection spectroscopy. (a) Reflectance magnitude $|r|$ as a function of probe frequency shows signature of both the state $|a\rangle$ at $\omega_a/2\pi = 5.6981$ GHz and state $|s\rangle$ at $\omega_s/2\pi = 6.2909$ GHz when probed from the waveguides A (upper panel) and S (lower panel). (b),(c) Plot of imaginary part versus real part of r for (b) state $|a\rangle$ probed in waveguide A and (c) state $|s\rangle$ probed in waveguide S at selected input powers. All solid lines are fits based on the model in Supplemental Material [63].

The input signals consist of a continuous-wave tone, a time-resolved probe tone, or their combination. The continuous tone is generated by microwave sources, called pumps in Fig. 1(c), whereas the time-resolved probe tones are tailored with a microwave transceiver used with in-phase-quadrature (IQ) mixers. The transceiver also acquires the signals from the output line as time traces. To perform coherent measurements, especially of population transfers (discussed below) between states $|a\rangle$ and $|s\rangle$ of different frequencies, it is vital to acquire the time traces with the same phase across multiple realizations (shots) of the experiment. This is enforced by driving all IQ mixers with the same local oscillator and a centralized transceiver. The Supplemental Material [63] provides more details.

We first measure the power-dependent reflectance r from both waveguides using a vector network analyzer (Fig. 2). It is strongly dependent on the coupling rate between each waveguide and the single-excitation state of corresponding symmetry, $\Gamma_{\{a,s\}}$, and the coupling rate of that state to any other decay channel, $\Gamma'_{\{a,s\}}$. When measured from waveguide A, $|r|$ exhibits a strong suppression at the mode frequency of $|a\rangle$, $\omega_a/2\pi$ at a power referred to as the “magic power” [64], a signature that the transition $|0\rangle \leftrightarrow |a\rangle$ is overcoupled to waveguide A ($\Gamma_a > \Gamma'_a$).

The suppression is due to destructive interference between reflected and coherently scattered radiation from a two-level system. A small dip (~ 0.3 dB) also appears at the mode frequency of $|s\rangle$, $\omega_s/2\pi$ at sufficiently low powers, indicating that the transition $|0\rangle \leftrightarrow |s\rangle$ is strongly undercoupled. When measuring r from waveguide S, we make opposite observations, i.e., we observe full suppression at $\omega_s/2\pi$ but only a small dip at $\omega_a/2\pi$ (Fig. 2(a), bottom). For the two overcoupled transitions, we measure the full power dependence of r and find that at low power r traces a nearly unit circle in the IQ plane, which continuously reduces toward a single point (+1) as the power is increased [Figs. 2(b) and 2(c)]. This trend reflects the transition between coherent and incoherent scattering as a two-level system is driven toward saturation [37]. The data is very well described by a two-level model based on the Lindblad master equation and input-output theory [15] (see Supplemental Material [63]). Based on global fits of the model [64,65] to the data, we extract the coupling rates $\Gamma_{\{a,s\}}$ and $\Gamma'_{\{a,s\}}$ (Table I). The fact that $\Gamma_s > \Gamma_a$ is owing to several factors, dominantly due to a strong capacitance between the inner nodes (coupling to the waveguide S), whose counterpart does not exist between the same-side nodes coupling to waveguide A. We find that $\Gamma'_{\{a,s\}}$ is largely the coupling to the waveguide of opposite symmetry because the corresponding r measurements can be fit fairly well by exchanging the values of $\Gamma_{\{a,s\}}$ and $\Gamma'_{\{a,s\}}$ (Fig. 2(a), insets). State $|a\rangle$ ($|s\rangle$) primarily emits into waveguide A (S) with a high coupling selectivity of $\Gamma_a/\Gamma'_a = 35$ ($\Gamma_s/\Gamma'_s = 47$). This is primarily attributed to the high electrostatic shielding of the waveguides from the unintended transmons’ nodes and engineered capacitance network in our device such that the voltage excitations of the collective states are localized as exclusively as possible in the expected nodes.

The selectivity in the emission properties of states with opposite symmetry is desirably complemented by a mechanism to activate a strong, coherent coupling between them. This is enabled by a Raman process between $|a\rangle$ and $|s\rangle$, mediated by the state $|2-\rangle$ [49,66,67] [Fig. 3(a)]. To do so, we send pump tones at frequency ω_- (ω_+) with pump amplitude Ω_- (Ω_+) to waveguide A (S). The Raman resonance occurs when $\omega_+ - \omega_- \approx \omega_s - \omega_a$ and, in the doubly rotated frame, causes the orthogonal states $|a\rangle$ and $|s\rangle$ to become resonant and couple with strength $\Omega_+ \Omega_- / 2\delta$ [49], where δ is the detuning between the virtual state of the Raman process and $|2-\rangle$. To observe the coupling, we study the transmission of weak coherent tones of frequency ω_p and drive amplitude Ω_p from waveguide S into waveguide A at the converted frequency $\omega_p + \omega_+ - \omega_-$ while the Raman process is activated with pumps. We fix $\delta/2\pi = 300$ MHz, a sufficient detuning to avoid direct population of the $|2-\rangle$ state. The measured power transmission, $|t|^2$, as a function of ω_p exhibits a clear peak,

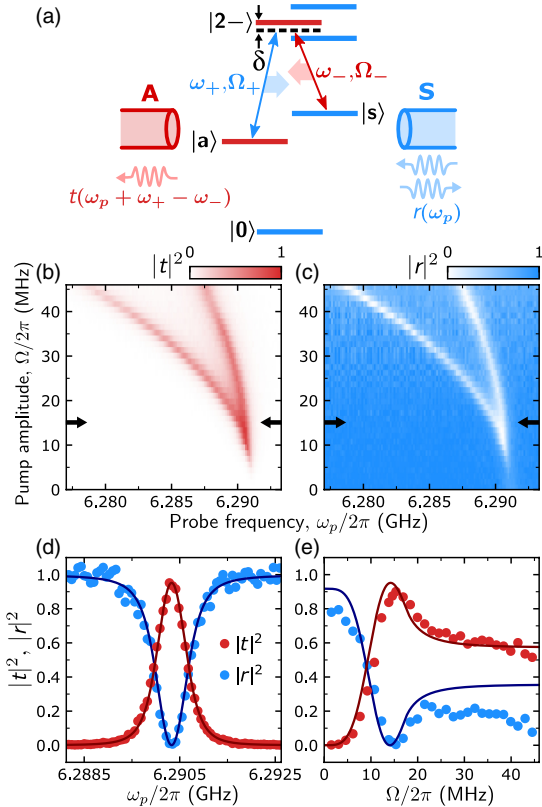


FIG. 3. Coupling and coherent population transfers between states of opposite symmetries using a Raman process. (a) Level diagram; see text for description. (b),(c) 2D plot of (b) power transmittance, $|t|^2$, and (c) power reflectance, $|r|^2$, as a function of probe frequency ω_p and pump amplitude $\Omega = \Omega_+ = \Omega_-$. (d) Plot of $|t|^2$ and $|r|^2$ at the optimal $\Omega/2\pi = 15.35$ MHz as a function of ω_p . (e) Plot of the maximum $|t|^2$ and correspondingly minimum $|r|^2$ as a function of Ω , when following the higher-frequency resonance in (b),(c). Solid lines in (d),(e) are theoretical predictions.

signifying Raman resonance, when the common pump amplitude $\Omega = \Omega_{+-}$ is sufficiently increased and reaches nearly 90.1% power transmission at $\Omega/2\pi = 15.35$ MHz [Fig. 3(b)]. Above this optimal value, Ω becomes large enough to split the resonant Raman levels that appear as two local maxima in $|t|^2$, while Stark shifting at the same time. The same trends are observed in the measured power reflection, $|r|^2$, which exhibits the corresponding minima where the Raman resonance occurs [Fig. 3(c)]. The efficiency of the population transfer is sensitive to the probe power used, which is about $\Omega_p/\Gamma_s = 0.116$ for the measurement of Figs. 3(b) and 3(c). When using a smaller probe amplitude, $\Omega_p/\Gamma_s = 0.077$, well in the linear response regime, the maximum $|t|^2$ reaches 95.2% [Fig. 3(d)]. $|r|^2$ diminishes to almost zero here, implying that less than 5% of power is lost incoherently during optimal population transfer. Beyond the optimal Ω , the maximum achievable $|t|^2$ decreases slowly with Ω

[Fig. 3(e)]. These results are in excellent agreement with a simple two-state model based on a non-Hermitian Hamiltonian, which uses only independently extracted spectroscopic parameters, without any fitting parameters (solid lines in Figs. 3(d) and 3(e); see Supplemental Material [63]). In Fig. 3(e), we note that $|r|^2$ is less than 1 for $\Omega \rightarrow 0$ because of nonzero direct scattering into the waveguide A ($\Gamma'_s/\Gamma_s > 0$, already captured by the model) and partial saturation of the state $|s\rangle$ due to a nonzero Ω_p chosen to be high enough for adequate signal to noise ratio. Deviations in $|r|^2$ from the model at large Ω may be accounted by a model incorporating other doubly excited states [see Fig. 1(b)]. We expect the demonstrated Raman process to transfer population in the reverse direction as well with comparable efficiency.

The V-shaped structure of the level diagram in Fig. 1(b) lends itself well to generating entanglement between the radiation emitted by the $|a\rangle \rightarrow |0\rangle$ and $|s\rangle \rightarrow |0\rangle$ transitions. Thanks to our waveguide engineering, this radiation is directly emitted into spatially separated modes. To demonstrate entanglement between propagating photonic modes, we enable the following sequence of events [Fig. 4(a)]: (1) induce a $\pi/2$ rotation between $|0\rangle$ and $|a\rangle$ by applying a resonant pulse of 80 ns duration to waveguide A; (2) induce a rotation of variable angle θ between $|0\rangle$ and $|s\rangle$ by applying a resonant pulse of duration 50 ns to waveguide S; and (3) let the molecule spontaneously decay, thereby transferring the original entanglement to propagating photonic modes. After the above sequence, we expect to find the system in the state

$$\frac{1}{\sqrt{2}}|0\rangle \left[\cos \frac{\theta}{2} |0\rangle_A |0\rangle_S + \left(\sin \frac{\theta}{2} |0\rangle_A |1\rangle_S + |1\rangle_A |0\rangle_S \right) \right],$$

where $|\{0, 1\}\rangle_{\{A, S\}}$ are Fock states of propagating modes in waveguides A and S, which, in the following, we describe by the annihilation operators \hat{a}_A and \hat{a}_S , respectively.

We perform tomographic reconstruction of selected moments of both photonic modes, $\hat{a}_{A,S}$, which are simultaneously read out as voltage signals at the output lines of both waveguides using our linear amplification chain and temporal mode matching, employing the techniques described in Ref. [68] (see Supplemental Material [63] for details). The whole measurement acquisition chain, including all its analog and digital gains, are calibrated by normalizing the $\hat{a}_{A,S}$ readouts with reference to values found for the photon fluxes, $\hat{a}_A^\dagger \hat{a}_A$ and $\hat{a}_S^\dagger \hat{a}_S$, at $\theta = \pi$, such that they scale to the theoretically expected value at $\theta = \pi$, having taken into account all observed decay processes and pulsed drives used in the experiment. We compare our results against a control experiment in which event (1) is omitted from the sequence [square data points in Figs. 4(b)–4(g)]. The measured first-order moments $\langle \hat{a}_A \rangle$ and $\langle \hat{a}_S \rangle$ [circle data points in Figs. 4(b) and 4(c)] are close to the calculated expectation values, $\langle \hat{a}_A \rangle = \frac{1}{2} \cos \theta/2$ and

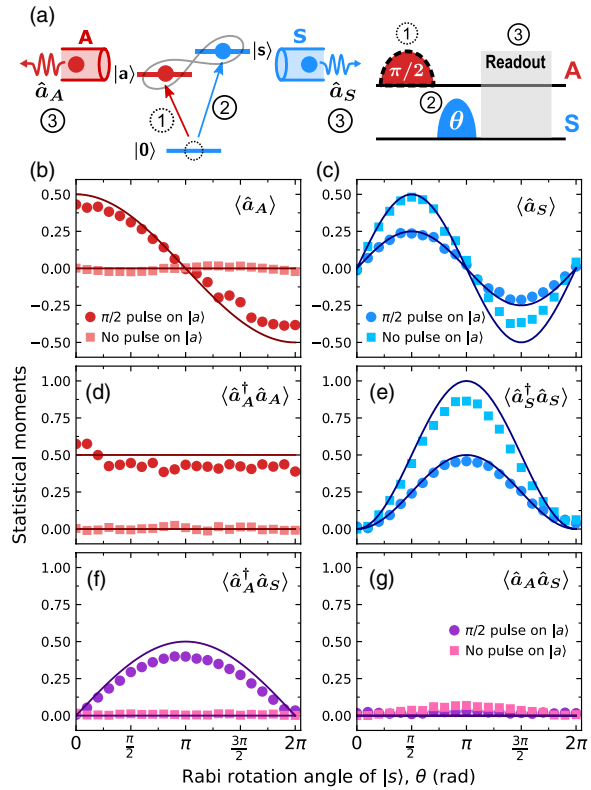


FIG. 4. Entanglement of propagating microwave fields in two separate waveguides. (a) (Left) Step sequence to entangle propagating fields in the waveguides A and S. (Right) Corresponding pulse sequence followed by simultaneous readouts in the output lines of both waveguides. The entanglement is conditional on the first step in which a $\pi/2$ pulse is sent to state $|a\rangle$; all results are compared against the case of its omission. (b)–(g) Selected moments of the photonic modes $\hat{a}_{\{A,S\}}$ in waveguides $\{A, S\}$ vs Rabi rotation angle θ of the pulse sent to waveguide S.

$\langle \hat{a}_S \rangle = \frac{1}{4} \sin \theta$ [solid lines in Figs. 4(b) and 4(c)]. However, the measurements deviate slightly from the ideal functional forms because the excitations decay during the pulsed drives owing to the short lifetimes of these states ($1/\Gamma_a = 512$ ns, $1/\Gamma_s = 115$ ns) and their small cross-coupling to the waveguide of the opposite symmetry. We expect the photon flux $\langle \hat{a}_A^\dagger \hat{a}_A \rangle$ to be 0.5, irrespective of θ [Fig. 4(d)], because event (1) drives the molecule to the superposition state $(|0\rangle + |a\rangle)/\sqrt{2}$. Subsequently, the molecule's state $|0\rangle$ is left with a population of nearly 0.5, available for coherent exchange with the state $|s\rangle$ when driven by the second pulse. Consequently, $\langle \hat{a}_S^\dagger \hat{a}_S \rangle$ oscillates up to an amplitude of nearly 0.5 as opposed to 1 in the case when event (1) is omitted because the population of state $|0\rangle$ is 1 to begin with [Fig. 4(e)].

The main signature of entanglement is encoded in the cross-moments, $\langle \hat{a}_A^\dagger \hat{a}_S \rangle$ and $\langle \hat{a}_A \hat{a}_S \rangle$ [Figs. 4(f) and 4(g)]. Only $\langle \hat{a}_A^\dagger \hat{a}_S \rangle$ takes a sufficiently large value when the $\pi/2$ pulse is applied to $|a\rangle$, reaching nearly 0.5 as expected for

the Bell state $(|01\rangle + |10\rangle)/\sqrt{2}$ at $\theta = \pi$ while obeying the functional form of the expectation value, $\langle \hat{a}_A^\dagger \hat{a}_S \rangle = \frac{1}{2} \sin \theta/2$. Moreover, a much smaller value of $\langle \hat{a}_A \hat{a}_S \rangle$ close to zero reassures the formation of this specific Bell state. The slight variation here is likely due to the cross-couplings noted above. While full quantum state tomography would be required in order to quantify the fidelity of the generated states [68], which we theoretically expect to be 89.4% for the Bell state, the measured data provide compelling evidence that the targeted process is realized in our system, given that resonant driving of a two-level system followed by spontaneous decay has been used to implement highly efficient single-photon sources in earlier works [69,70].

In summary, we have presented a novel waveguide QED architecture in which transitions in a diatomic artificial molecule are selectively coupled to two waveguides, depending on their inherent symmetries. The selective coupling mechanism is implanted in the device and requires no static or dynamic tuning of frequencies or phase differences in control pulses [18,48]. We have provided two examples of the capabilities of this architecture: a coherent frequency converter operating between states of opposite symmetries with efficiency close to unity, and a simple scheme to generate maximally entangled propagating modes in spatially separate waveguides. A number of further applications can be envisaged. Setting one of the two waveguides in the undercoupling regime enables the creation of a long-lived metastable state, which can be coupled to the bright state either coherently, via a Raman process, or irreversibly via a resonant coupling to the second-excitation manifold followed by photon emission into the strongly coupled waveguide. The latter scheme leads to an impedance-matched lambda system that can be exploited for photodetection [71–73]. A scheme similar to the one used to generate Bell states may be used to realize photon-photon gates [74] across separate waveguides. When the waveguides are populated with thermal fields [37,38], and the dark and bright states are coherently coupled by demonstrated Raman process, the molecule operates as a quantum thermal machine (heat engine or refrigerator), paving the way for studies in quantum thermodynamics. Finally, the presented scheme can be extended to larger artificial molecules, arrays of qubits or resonators [75], and generally to any other physical system with near-field coupling to an electric or magnetic dipole—for example, double quantum dots [76].

We are grateful to Francesco Ciccarello, Giuseppe Calajò, and Anton Frisk Kockum for useful feedback to our results. The presented device was fabricated in Myfab Chalmers, a nanofabrication laboratory, and its design was assisted by the PYTHON package QuCAT [77]. We acknowledge financial support from Swedish Research Council and the Knut and Alice Wallenberg Foundation through the Wallenberg Center for Quantum Technology (WACQT).

*Corresponding author.

aamir.ali@chalmers.se

[†]Corresponding author.

simoneg@chalmers.se; www.202q-lab.se

- [1] A. S. Sheremet, M. I. Petrov, I. V. Iorsh, A. V. Poshakinskiy, and A. N. Poddubny, Waveguide quantum electrodynamics: Collective radiance and photon-photon correlations, [arXiv:2103.06824](https://arxiv.org/abs/2103.06824).
- [2] D. Roy, C. M. Wilson, and O. Firstenberg, Colloquium: Strongly interacting photons in one-dimensional continuum, *Rev. Mod. Phys.* **89**, 021001 (2017).
- [3] P. Lodahl, S. Mahmoodian, and S. Stobbe, Interfacing single photons and single quantum dots with photonic nanostructures, *Rev. Mod. Phys.* **87**, 347 (2015).
- [4] X. Gu, A. F. Kockum, A. Miranowicz, Y.-x. Liu, and F. Nori, Microwave photonics with superconducting quantum circuits, *Phys. Rep.* **718–719**, 1 (2017).
- [5] N. V. Corzo, J. Raskop, A. Chandra, A. S. Sheremet, B. Gouraud, and J. Laurat, Waveguide-coupled single collective excitation of atomic arrays, *Nature (London)* **566**, 359 (2019).
- [6] A. Sipahigil, R. E. Evans, D. D. Sukachev, M. J. Burek, J. Borregaard, M. K. Bhaskar, C. T. Nguyen, J. L. Pacheco, H. A. Atikian, C. Meuwly, R. M. Camacho, F. Jelezko, E. Bielejec, H. Park, M. Lončar, and M. D. Lukin, An integrated diamond nanophotonics platform for quantum-optical networks, *Science* **354**, 847 (2016).
- [7] A. P. Foster, D. Hallett, I. V. Iorsh, S. J. Sheldon, M. R. Godsland, B. Royall, E. Clarke, I. A. Shelykh, A. M. Fox, M. S. Skolnick, I. E. Itskevich, and L. R. Wilson, Tunable Photon Statistics Exploiting the Fano Effect in a Waveguide, *Phys. Rev. Lett.* **122**, 173603 (2019).
- [8] M. Mirhosseini, E. Kim, X. Zhang, A. Sipahigil, P. B. Dieterle, A. J. Keller, A. Asenjo-Garcia, D. E. Chang, and O. Painter, Cavity quantum electrodynamics with atom-like mirrors, *Nature (London)* **569**, 692 (2019).
- [9] O. Astafiev, A. M. Zagoskin, A. A. Abdumalikov, Jr., Y. A. Pashkin, T. Yamamoto, K. Inomata, Y. Nakamura, and J. S. Tsai, Resonance fluorescence of a single artificial atom, *Science* **327**, 840 (2010).
- [10] I.-C. Hoi, T. Palomaki, J. Lindkvist, G. Johansson, P. Delsing, and C. M. Wilson, Generation of Nonclassical Microwave States Using an Artificial Atom in 1D Open Space, *Phys. Rev. Lett.* **108**, 263601 (2012).
- [11] Y. Lu, I. Strandberg, F. Quijandría, G. Johansson, S. Gasparinetti, and P. Delsing, Propagating Wigner-Negative States Generated from the Steady-State Emission of a Superconducting Qubit, *Phys. Rev. Lett.* **126**, 253602 (2021).
- [12] R. G. DeVoe and R. G. Brewer, Observation of Superradiant and Subradiant Spontaneous Emission of Two Trapped Ions, *Phys. Rev. Lett.* **76**, 2049 (1996).
- [13] W. Guerin, M. O. Araujo, and R. Kaiser, Subradiance in a Large Cloud of Cold Atoms, *Phys. Rev. Lett.* **116**, 083601 (2016).
- [14] P. Solano, P. Barberis-Blostein, F. K. Fatemi, L. A. Orozco, and S. L. Rolston, Super-radiance reveals infinite-range dipole interactions through a nanofiber, *Nat. Commun.* **8**, 1857 (2017).
- [15] K. Lalumière, B. C. Sanders, A. F. van Loo, A. Fedorov, A. Wallraff, and A. Blais, Input-output theory for waveguide QED with an ensemble of inhomogeneous atoms, *Phys. Rev. A* **88**, 043806 (2013).
- [16] A. van Loo, A. Fedorov, K. Lalumière, B. Sanders, A. Blais, and A. Wallraff, Photon-mediated interactions between distant artificial atoms, *Science* **342**, 1494 (2013).
- [17] S. J. Masson and A. Asenjo-Garcia, Atomic-waveguide quantum electrodynamics, *Phys. Rev. Research* **2**, 043213 (2020).
- [18] M. Zanner, T. Orell, C. M. F. Schneider, R. Albert, S. Oleschko, M. L. Juan, M. Silveri, and G. Kirchmair, Coherent control of a multi-qubit dark state in waveguide quantum electrodynamics, *Nat. Phys.* **18**, 538 (2022).
- [19] A. F. Kockum, G. Johansson, and F. Nori, Decoherence-Free Interaction between Giant Atoms in Waveguide Quantum Electrodynamics, *Phys. Rev. Lett.* **120**, 140404 (2018).
- [20] B. Kannan, M. J. Ruckriegel, D. L. Campbell, A. Frisk Kockum, J. Braumüller, D. K. Kim, M. Kjaergaard, P. Krantz, A. Melville, B. M. Niedzielski, A. Vepsäläinen, R. Winik, J. L. Yoder, F. Nori, T. P. Orlando, S. Gustavsson, and W. D. Oliver, Waveguide quantum electrodynamics with superconducting artificial giant atoms, *Nature (London)* **583**, 775 (2020).
- [21] A. M. Vadiraj, A. Ask, T. G. McConkey, I. Nsanzineza, C. W. Sandbo Chang, A. F. Kockum, and C. M. Wilson, Engineering the level structure of a giant artificial atom in waveguide quantum electrodynamics, *Phys. Rev. A* **103**, 023710 (2021).
- [22] P. Lodahl, S. Mahmoodian, S. Stobbe, A. Rauschenbeutel, P. Schneeweiss, J. Volz, H. Pichler, and P. Zoller, Chiral quantum optics, *Nature (London)* **541**, 473 (2017).
- [23] M. Scheucher, A. Hilico, E. Will, J. Volz, and A. Rauschenbeutel, Quantum optical circulator controlled by a single chirally coupled atom, *Science* **354**, 1577 (2016).
- [24] S. Mahmoodian, G. Calajó, D. E. Chang, K. Hammerer, and A. S. Sørensen, Dynamics of Many-Body Photon Bound States in Chiral Waveguide QED, *Phys. Rev. X* **10**, 031011 (2020).
- [25] N. Gheeraert, S. Kono, and Y. Nakamura, Programmable directional emitter and receiver of itinerant microwave photons in a waveguide, *Phys. Rev. A* **102**, 053720 (2020).
- [26] P. O. Guimond, B. Vermersch, M. L. Juan, A. Sharafiev, G. Kirchmair, and P. Zoller, A unidirectional on-chip photonic interface for superconducting circuits, *npj Quantum Inf.* **6**, 32 (2020).
- [27] Y. Liu and A. A. Houck, Quantum electrodynamics near a photonic bandgap, *Nat. Phys.* **13**, 48 (2016).
- [28] M. Mirhosseini, E. Kim, V. S. Ferreira, M. Kalaei, A. Sipahigil, A. J. Keller, and O. Painter, Superconducting metamaterials for waveguide quantum electrodynamics, *Nat. Commun.* **9**, 3706 (2018).
- [29] N. M. Sundaresan, R. Lundgren, G. Zhu, A. V. Gorshkov, and A. A. Houck, Interacting Qubit-Photon Bound States with Superconducting Circuits, *Phys. Rev. X* **9**, 011021 (2019).
- [30] J. D. Brehm, A. N. Poddubny, A. Stehli, T. Wolz, H. Rotzinger, and A. V. Ustinov, Waveguide bandgap engineering with an array of superconducting qubits, *npj Quantum Mater.* **6**, 10 (2021).

- [31] E. Kim, X. Zhang, V. S. Ferreira, J. Bunker, J. K. Iverson, A. Sipahigil, M. Bello, A. González-Tudela, M. Mirhosseini, and O. Painter, Quantum Electrodynamics in a Topological Waveguide, *Phys. Rev. X* **11**, 011015 (2021).
- [32] I. S. Besedin, M. A. Gorlach, N. N. Abramov, I. Tsitsilin, I. N. Moskalenko, A. A. Dobronosova, D. O. Moskalev, A. R. Matanin, N. S. Smirnov, I. A. Rodionov, A. N. Poddubny, and A. V. Ustinov, Topological excitations and bound photon pairs in a superconducting quantum metamaterial, *Phys. Rev. B* **103**, 224520 (2021).
- [33] G. Andersson, B. Suri, L. Guo, T. Aref, and P. Delsing, Non-exponential decay of a giant artificial atom, *Nat. Phys.* **15**, 1123 (2019).
- [34] V. S. Ferreira, J. Bunker, A. Sipahigil, M. H. Matheny, A. J. Keller, E. Kim, M. Mirhosseini, and O. Painter, Collapse and Revival of an Artificial Atom Coupled to a Structured Photonic Reservoir, *Phys. Rev. X* **11**, 041043 (2021).
- [35] B. Kannan, D. L. Campbell, F. Vasconcelos, R. Winik, D. K. Kim, M. Kjaergaard, P. Krantz, A. Melville, B. M. Niedzielski, J. L. Yoder, T. P. Orlando, S. Gustavsson, and W. D. Oliver, Generating spatially entangled itinerant photons with waveguide quantum electrodynamics, *Sci. Adv.* **6**, eabb8780 (2020).
- [36] N. Cottet, S. Jezouin, L. Bretheau, P. Campagne-Ibarcq, Q. Ficheux, J. Anders, A. Auffèves, R. Azouit, P. Rouchon, and B. Huard, Observing a quantum Maxwell demon at work, *Proc. Natl. Acad. Sci. U.S.A.* **114**, 7561 (2017).
- [37] M. Scigliuzzo, A. Bengtsson, J.-C. Besse, A. Wallraff, P. Delsing, and S. Gasparinetti, Primary Thermometry of Propagating Microwaves in the Quantum Regime, *Phys. Rev. X* **10**, 041054 (2020).
- [38] Y. Lu, N. Lambert, A. F. Kockum, K. Funo, A. Bengtsson, S. Gasparinetti, F. Nori, and P. Delsing, Steady-state heat transport and work with a single artificial atom coupled to a waveguide: Emission without external driving, *PRX Quantum* **3**, 020305 (2022).
- [39] J. Monsel, M. Fellous-Asiani, B. Huard, and A. Auffèves, The Energetic Cost of Work Extraction, *Phys. Rev. Lett.* **124**, 130601 (2020).
- [40] R. H. Dicke, Coherence in spontaneous radiation processes, *Phys. Rev.* **93**, 99 (1954).
- [41] A. González-Tudela and D. Porras, Mesoscopic Entanglement Induced by Spontaneous Emission in Solid-State Quantum Optics, *Phys. Rev. Lett.* **110**, 080502 (2013).
- [42] J. Mlynek, A. Abdumalikov, C. Eichler, and A. Wallraff, Observation of Dicke superradiance for two artificial atoms in a cavity with high decay rate, *Nat. Commun.* **5**, 5186 (2014).
- [43] T. Monz, K. Kim, A. S. Villar, P. Schindler, M. Chwalla, M. Riebe, C. F. Roos, H. Häffner, W. Hänsel, M. Hennrich, and R. Blatt, Realization of Universal Ion-Trap Quantum Computation with Decoherence-Free Qubits, *Phys. Rev. Lett.* **103**, 200503 (2009).
- [44] D. Kielpinski, V. Meyer, M. Rowe, C. Sackett, W. Itano, C. Monroe, and D. Wineland, A decoherence-free quantum memory using trapped ions, *Science* **291**, 1013 (2001).
- [45] V. Paulisch, H. J. Kimble, and A. González-Tudela, Universal quantum computation in waveguide QED using decoherence free subspaces, *New J. Phys.* **18**, 043041 (2016).
- [46] D. A. Lidar, I. L. Chuang, and K. B. Whaley, Decoherence-Free Subspaces for Quantum Computation, *Phys. Rev. Lett.* **81**, 2594 (1998).
- [47] P. M. Leung and B. C. Sanders, Coherent Control of Microwave Pulse Storage in Superconducting Circuits, *Phys. Rev. Lett.* **109**, 253603 (2012).
- [48] S. Filipp, A. F. van Loo, M. Baur, L. Steffen, and A. Wallraff, Preparation of subradiant states using local qubit control in circuit QED, *Phys. Rev. A* **84**, 061805(R) (2011).
- [49] C. C. Gerry and J. H. Eberly, Dynamics of a Raman coupled model interacting with two quantized cavity fields, *Phys. Rev. A* **42**, 6805 (1990).
- [50] N. Roch, E. Flurin, F. Nguyen, P. Morfin, P. Campagne-Ibarcq, M. H. Devoret, and B. Huard, Widely Tunable, Nondegenerate Three-Wave Mixing Microwave Device Operating near the Quantum Limit, *Phys. Rev. Lett.* **108**, 147701 (2012).
- [51] E. P. Menzel, R. Di Candia, F. Deppe, P. Eder, L. Zhong, M. Ihmig, M. Haeberlein, A. Baust, E. Hoffmann, D. Ballester, K. Inomata, T. Yamamoto, Y. Nakamura, E. Solano, A. Marx, and R. Gross, Path Entanglement of Continuous-Variable Quantum Microwaves, *Phys. Rev. Lett.* **109**, 250502 (2012).
- [52] E. Flurin, N. Roch, F. Mallet, M. H. Devoret, and B. Huard, Generating Entangled Microwave Radiation Over Two Transmission Lines, *Phys. Rev. Lett.* **109**, 183901 (2012).
- [53] S. Gasparinetti, M. Pechal, J.-C. Besse, M. Mondal, C. Eichler, and A. Wallraff, Correlations and Entanglement of Microwave Photons Emitted in a Cascade Decay, *Phys. Rev. Lett.* **119**, 140504 (2017).
- [54] A. Peugeot, G. Ménard, S. Dambach, M. Westig, B. Kubala, Y. Mukharsky, C. Altimiras, P. Joyez, D. Vion, P. Roche, D. Esteve, P. Milman, J. Leppäkangas, G. Johansson, M. Hofheinz, J. Ankerhold, and F. Portier, Generating Two Continuous Entangled Microwave Beams Using a dc-Biased Josephson Junction, *Phys. Rev. X* **11**, 031008 (2021).
- [55] A. Narla, S. Shankar, M. Hatridge, Z. Leghtas, K. M. Sliwa, E. Zalys-Geller, S. O. Mundhada, W. Pfaff, L. Frunzio, R. J. Schoelkopf, and M. H. Devoret, Robust Concurrent Remote Entanglement Between Two Superconducting Qubits, *Phys. Rev. X* **6**, 031036 (2016).
- [56] P. Kurpiers, P. Magnard, T. Walter, B. Royer, M. Pechal, J. Heinsoo, Y. Salathé, A. Akin, S. Storz, J.-C. Besse, S. Gasparinetti, A. Blais, and A. Wallraff, Deterministic quantum state transfer and remote entanglement using microwave photons, *Nature (London)* **558**, 264 (2018).
- [57] C. Axline, L. Burkhardt, W. Pfaff, M. Zhang, K. Chou, P. Campagne-Ibarcq, P. Reinhold, L. Frunzio, S. M. Girvin, L. Jiang, M. H. Devoret, and R. J. Schoelkopf, On-demand quantum state transfer and entanglement between remote microwave cavity memories, *Nat. Phys.* **14**, 705 (2018).
- [58] P. Campagne-Ibarcq, E. Zalys-Geller, A. Narla, S. Shankar, P. Reinhold, L. Burkhardt, C. Axline, W. Pfaff, L. Frunzio, R. J. Schoelkopf, and M. H. Devoret, Deterministic Remote Entanglement of Superconducting Circuits through Microwave Two-Photon Transitions, *Phys. Rev. Lett.* **120**, 200501 (2018).
- [59] J. Koch, T. M. Yu, J. Gambetta, A. A. Houck, D. I. Schuster, J. Majer, A. Blais, M. H. Devoret, S. M. Girvin, and R. J.

- Schoelkopf, Charge-insensitive qubit design derived from the Cooper pair box, *Phys. Rev. A* **76**, 042319 (2007).
- [60] S. Filipp, M. Göppl, J. M. Fink, M. Baur, R. Bianchetti, L. Steffen, and A. Wallraff, Multimode mediated qubit-qubit coupling and dark-state symmetries in circuit quantum electrodynamics, *Phys. Rev. A* **83**, 063827 (2011).
- [61] A. Crubellier, S. Liberman, D. Pavolini, and P. Pillet, Superradiance and subradiance. I. Interatomic interference and symmetry properties in three-level systems, *J. Phys. B* **18**, 3811 (1985).
- [62] T. K. Begzjav, L. Wang, and R. Nessler, On permutation symmetry of subradiant states and its application, *Phys. Scr.* **94**, 094001 (2019).
- [63] See Supplemental Material at <http://link.aps.org/supplemental/10.1103/PhysRevLett.129.123604> for more details of the experimental setup, measurements, energy levels and their transitions, and relevant theoretical models.
- [64] I.-C. Hoi, A. F. Kockum, L. Tornberg, A. Pourkabirian, G. Johansson, P. Delsing, and C. M. Wilson, Probing the quantum vacuum with an artificial atom in front of a mirror, *Nat. Phys.* **11**, 1045 (2015).
- [65] Y. Lu, A. Bengtsson, J. J. Burnett, E. Wiegand, B. Suri, P. Krantz, A. F. Roudsari, A. F. Kockum, S. Gasparinetti, G. Johansson, and P. Delsing, Characterizing decoherence rates of a superconducting qubit by direct microwave scattering, *npj Quantum Inf.* **7**, 1 (2021).
- [66] K. Bergmann, H. Theuer, and B. W. Shore, Coherent population transfer among quantum states of atoms and molecules, *Rev. Mod. Phys.* **70**, 1003 (1998).
- [67] K. S. Kumar, A. Vepsäläinen, S. Danilin, and G. S. Paraoanu, Stimulated Raman adiabatic passage in a three-level superconducting circuit, *Nat. Commun.* **7**, 10628 (2016).
- [68] C. Eichler, D. Bozyigit, C. Lang, L. Steffen, J. Fink, and A. Wallraff, Experimental State Tomography of Itinerant Single Microwave Photons, *Phys. Rev. Lett.* **106**, 220503 (2011).
- [69] Z. H. Peng, S. E. de Graaf, J. S. Tsai, and O. V. Astafiev, Tuneable on-demand single-photon source in the microwave range, *Nat. Commun.* **7**, 12588 (2016).
- [70] M. Pechal, J.-C. Besse, M. Mondal, M. Oppliger, S. Gasparinetti, and A. Wallraff, Superconducting Switch for Fast On-Chip Routing of Quantum Microwave Fields, *Phys. Rev. Applied* **6**, 024009 (2016).
- [71] K. Koshino, K. Inomata, T. Yamamoto, and Y. Nakamura, Implementation of an Impedance-Matched Λ System by Dressed-State Engineering, *Phys. Rev. Lett.* **111**, 153601 (2013).
- [72] K. Inomata, Z. Lin, K. Koshino, W. D. Oliver, J. Tsai, T. Yamamoto, and Y. Nakamura, Single microwave-photon detector using an artificial Λ -type three-level system, *Nat. Commun.* **7**, 12303 (2016).
- [73] R. Lescanne, S. Deléglise, E. Albertinale, U. Réglade, T. Capelle, E. Ivanov, T. Jacqmin, Z. Leghtas, and E. Flurin, Irreversible Qubit-Photon Coupling for the Detection of Itinerant Microwave Photons, *Phys. Rev. X* **10**, 021038 (2020).
- [74] K. Reuer, J.-C. Besse, L. Wernli, P. Magnard, P. Kurpiers, G. J. Norris, A. Wallraff, and C. Eichler, Realization of a Universal Quantum Gate Set for Itinerant Microwave Photons, *Phys. Rev. X* **12**, 011008 (2022).
- [75] Y. Yanay, J. Braumüller, T. P. Orlando, S. Gustavsson, C. Tahan, and W. D. Oliver, Mediated Interactions beyond the Nearest Neighbor in an Array of Superconducting Qubits, *Phys. Rev. Applied* **17**, 034060 (2022).
- [76] A. Stockklauser, P. Scarlino, J. V. Koski, S. Gasparinetti, C. K. Andersen, C. Reichl, W. Wegscheider, T. Ihn, K. Ensslin, and A. Wallraff, Strong Coupling Cavity QED with Gate-Defined Double Quantum Dots Enabled by a High Impedance Resonator, *Phys. Rev. X* **7**, 011030 (2017).
- [77] M. F. Gely and G. A. Steele, QuCAT: Quantum circuit analyzer tool in Python, *New J. Phys.* **22**, 013025 (2020).